Relation between the interaction potential, replacement collision sequences, and collision cascade expansion in iron

C. S. Becquart
Laboratoire de Métallurgie Physique et Génie des Matériaux, USTL, CNRS UMR 8517, Bât. C6, F-59655 Villeneuve d'Ascq Cedex, France

A. Souidi
Centre Universitaire de Saida, BP138, En-nasr, Saida 20000, Algeria

M. Hou
Physique des Solides Irradiés CP234, Université Libre de Bruxelles, Bd du Triomphe, B-1050 Brussels, Belgium

(Received 27 March 2002; revised manuscript received 19 August 2002; published 23 October 2002)

The binary collision approximation (BCA) grounded on molecular dynamics results is used to investigate the influence of the range and stiffness of interatomic potentials on the replacement collision sequence (RCS) length and frequency distributions as well as on the displacement cascade expansion and density. Different screened Coulomb potential functions are used in the Marlowe BCA program with suitably adjusted screening lengths. We show in this paper that for screened Coulomb potentials, the shorter the range, the lower the focusing threshold and the more important the RCS production. The cascade expansion and density is quite sensitive to the potential range at high interaction energies. The overall cascade expansion is found to be governed by the 10% highest-energy recoils. Their energy is above the RCS focusing energy threshold. The cascade density, i.e., the number of transient defects produced per unit volume, is suggested sufficient to interfere significantly with RCS propagation and thus with the spatial distribution of Frenkel pairs. Primary damage production thus involves the combined effect of high-energy collisions and RCS production. A careful choice of the short range potential has thus to be made when simulating displacement cascades.

DOI: 10.1103/PhysRevB.66.134104 PACS number(s): 61.80.Az, 02.70.Ns, 61.82.Bg, 61.80.Lj

I. INTRODUCTION

Although radiation damage has been studied at the atomic scale for more than 40 years, it is still, nowadays, far from fully understood. Two methods have frequently been used to investigate the primary damage at the atomic level: molecular dynamics (MD) and its binary collision approximation (BCA). Accumulating statistics over large samples of collision cascades using full MD is nowadays unpractical in the energy ranges of interest for radiation damage studies. Indeed, to our knowledge, only a few hundred cascades are presently available in Fe, involving different temperatures and primary knocked-on atom (PKA) energies. A huge effort is presently ongoing to construct a database of these cascades in the framework of the International REVE project, a project which aims at simulating irradiation effects in structural materials.[1] This drawback is drastically reduced by the BCA of MD, on the expense of an approximate treatment of multiple simultaneous interactions. The BCA is several orders of magnitude less time consuming than MD and it therefore allows reasonably significant statistics in the case of broad statistical distributions. The consequences of the approximate treatment of simultaneous events are not all fully identified. However, the BCA can be grounded on MD results.[2–4] Such an approach has been used in the past to investigate the origin and importance of the variance in several properties characterizing atomic collision cascades in crystals and polycrystals.[5] In that work, the systematic comparison between MD and its BCA also allowed distinguishing ballistic from post-ballistic effects. In this respect, vacancy clusters formed during the ballistic phase of the cascades were identified to fragment as a consequence of the post-ballistic mixing (not predicted by the BCA) in the core of the cascades.[4]

The potential model is crucial in predicting primary damage. This was illustrated, among other examples, by MD simulations of displacement cascades in iron with three different model potentials published in the literature as representative models for Fe. It was found that the spatial distribution of primary damage is very sensitive to the potential.[6] Figure 1 is a typical example of the influence of the potential on the cascade morphology. In this example, which is typical of all other cascades computed in iron in an energy range from 1 keV to 20 keV with the same potentials (a total of around 60 cascades), it clearly appears that one of the Fe potential predicts very dilute cascades with long replacement collision sequences (RCS's), while the other produces more compact cascades. It has been recognized for some time that the primary state of damage is controlled at least by three phenomena: RCS's during the ballistic phase, mixing, and resolidification characterizing the cooling phases.[7] RCS's possibly transport interstitials beyond the core region before mixing starts. It has been observed many times that among the interstitials, mainly those that are created outside the melted core survive recombination. The multiple interaction nature of replacement sequences in face-centred-cubic metals has been analyzed in detail,[8–12] and a method to correct the BCA predictions with the help of MD simulations for the energy loss in RCS's was proposed.[3] A complementary work on the RCS mechanisms in bcc Fe and the influence of tem-

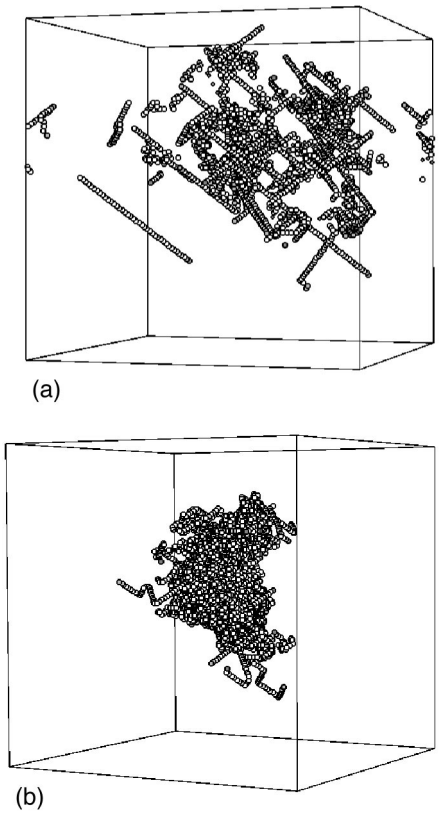

FIG. 1. Cascade morphology: replaced atoms of Fe II (a) and Fe I (b) EAM potentials for a 20 keV MD cascade at 600 K at the end of the displacement cascade.

perature can be found in another article.[13] This later study, which also grounds the BCA model on MD results, suggested that most linear collision sequences are short. Other BCA simulations showed that, probably, therefore, their length distributions and frequency of occurrence are not significantly temperature dependent.[14] This agrees with previous MD results showing that the drift temperature dependence of the residual defects and the defect clustering fraction is weak.[15] This has been confirmed in further MD studies by Gao and co-workers.[16] Hence, although RCS's involve many-body interactions, their contribution to the cascade development may be well predicted by a suitable BCA model.

Previous work seems to indicate that it is the short-distance interaction branch of the potential which is the most responsible for the differences in cascade morphologies like those in Fig. 1.[6,17] Indeed, the energies involved in RCS's are typically of the order of a few ten eV, and the initiation of RCS is thus governed by the short-distance interaction part of the potential. The question of the displacement cascade density and morphology seems to be also related to the short-distance portion of the potential, as the differences mentioned above appear very early on in the cascade development. The present work investigates thus the influence of the range and stiffness of repulsive potential branches on the RCS length and distribution as well as on the cascade expansion and density.

To address these questions in detail, we use BCA potentials parametrized so as to be close to the three interatomic potentials the influence of which on the simulation of the primary damage was investigated in a previous article.[6] As the Marlowe package provides a large variety of pair potential functions, it is straighforward to use several of them for modeling atomic collisions in iron. Building interatomic potentials for Fe suitable for MD simulations, even simple pair potentials, is not a trivial task, and a systematic study of the influence of the potential range and stiffness on the results requires good statistics (in this work, the generation of more than 100 000 BCA cascades was necessary).

The paper is organized as follows. In a first part we introduce concisely MD and its BCA approximation as well as the different potentials used in this work to simulate displacement cascades. The cascade expansion is characterized using the component analysis technique which is briefly reminded. Before investigating systematically the role of the range and stiffness of the BCA potentials on the RCS production, we briefly present the characteristics of the MD potentials usually connected with this aspect of the primary damage. Finally we address the question of which factors determine the cascade volume and density.

II. ATOMIC-SCALE MODELS

A. Potentials

Whatever the model, the basic parameter in describing atomic collision cascades is the potential from which forces derive. Since, in practice, collision cascades involve too large systems to be described quantum mechanically, potentials are established semiempirically. It turns out that the potential functions used nowadays are of two completely different origins, depending upon whether the equations of motion of the atoms are solved simultaneously or by means of the BCA. In the former approach (MD), a system is considered as a whole and the evolution of its solid state toward equilibrium is followed stepwise in time. The movement of each atom is governed by its global environment. In the latter, collision cascades are approximated by sequences of binary encounters that are not influenced by the environment. This approximation is too strong for slow particles in condensed matter but, as suggested below, simple models may significantly improve the situation. Traditionally, many-body potentials used to describe global environments are grounded on solid-state properties of materials while binary encounter potentials are grounded on statistical models of the atoms. We now consider these families distinctly. In the many-body approach, the force on an atom is derived from the configurational energy of the whole solid. This energy is expressed as a sum of two terms

$$E_c = \sum_i \varphi\left[\sum_j f(r_{ij})\right] + \frac{1}{2}\sum_{i,j} \phi(r_{ij}), \qquad (2.1)$$

where r_{ij} is the vector joining atom i to atom j, f is a pair function which describes the local environment, φ is a function describing how the energy of atom i depends on its environment, and ϕ is a repulsive pair potential. The repul-

sive term ϕ accounts for the Pauli exclusion principle and the electronic interaction between nuclei. It is often taken as a Born-Mayer exponential function. The environmental function in Eq. (2.1) may be derived from the tight-binding model where the attraction between atoms results from the broadening of partially filled valence orbitals into bands: in this model, φ is expressed in terms of moments of the density of states and the expansion is generally limited to the second moment.[18] The function φ can also be conveniently grounded on the so-called embedded atom model (EAM),[19] in which the binding energy of an atom is regarded as the energy gained by the system when this atom is embedded into the local electronic background density of all the other atoms. It is assumed that this function is made from the superposition of pairwise interactions. Whatever the approach used, Eq. (2.1) is usually parametrized on the basis of elastic constants, the cohesive energy, the vacancy formation energy, the lattice parameters, and other quantities representative of the equilibrium solid state involving characteristic interatomic distances of the order of 2 Å . Potentials used in the BCA are traditionally designed for close encounters and they account for electrostatic repulsion between nuclei and for the screening by the atomic electron distribution, which is usually neglected in potentials based on Eq. (2.1). The screening function was derived from the Thomas-Fermi statistical model of the atom.[20] This function was approximated by Molière who used the screening length[21]

$$a_{TF}=\left(\frac{9\pi^2}{128}\right)^{1/3} a_B Z^{-1/3}, \tag{2.2}$$

where Z is the atomic number and $a_B=0.52$ Å is the Bohr radius. For heteronuclear interactions, Z is often approximated by

$$Z=(Z_1^k+Z_2^k)^{k'}, \tag{2.3}$$

where $k=2$ or $k=3/2$ with $k'=1/k$ according to Firsov[22] and Lindhard *et al.*[23] respectively, or $k=0.23$ and $k'=3$ according to Ziegler and co-workers.[24] The screening length is also often used as a parameter. Whatever its expression, most of the available close encounter potentials can be written as

$$V(r)=\frac{Z_1 Z_2}{r}\phi\left(\frac{r}{a}\right), \tag{2.4}$$

with

$$\phi\left(\frac{r}{a}\right)=\sum \alpha_j \exp\left(-\beta_j \frac{r}{a}\right). \tag{2.5}$$

In the Molière version, $n=3$, while $n=4$ in the Ziegler version. The latter is often referred to as the ''universal'' or the Ziegler-Biersack-Littmark (ZBL) potential. The ZBL function results from a huge series of quantum mechanical interaction energy estimates, using nonrelativistic Hartree-Fock atomic wave functions. Using a similar approach, but including relativistic corrections, leads to the so-called ''average modified Lenz-Jensens'' potential (AMLJ) where the screening function may be written as[25]

$$\phi(r)=\exp(-\alpha_1 r+\alpha_2 r^{3/2}+\alpha_3 r^2). \tag{2.6}$$

The coefficients α_1, α_2, and α_3 are given by Robinson *et al.*[26]

For the BCA calculations presented in this work, we generally use the Molière potential systematically, taking the screening length as a parameter. The Born-Mayer potential is used when appropriate. It is given by

$$V(r)=A\exp\left(-\frac{r}{a_{12}}\right), \tag{2.7}$$

with $A=6893.87$ eV and where the screening distance a_{12} is also taken as a parameter.

The many-body potentials previously investigated in MD calculations of displacement cascades[6] are used in the present work as well and they will be referred to as Fe I, Fe II, and Fe III. They will serve to ground the BCA RCS model on MD. These potentials have been published elsewhere and the forms for the different functions can be found in the original publications. Fe I is a potential derived by Harrison and co-workers[27] (potential labeled FEB in Ref. 27). It was initially designed for interaction distances greater than 0.1 nm. Fe II is a potential derived by Haftel and co-workers[28] (potential labeled 4 in Ref. 28). Fe III was derived by Simonelli and co-workers.[29] To make these potentials suitable for displacement cascade simulation, it is necessary to modify the short-range part corresponding to close encounters. Most of the hardening efforts are concentrated on the pair components since the scattering is expected to be dominated by the repulsive part of the potential. For these components, one usually uses at short range (r less than 1 Å) screened Coulomb potentials such as the ZBL potential. For intermediate ranges, one typically utilizes Born-Mayer-type potentials similar to that published by Maury *et al.*[30] to give the appropriate threshold displacement energies. All these functions are joined by smooth interpolation schemes. Continuity between different branches is ensured at the knot points up to their first derivatives. The electron density and the embedding modification schemes vary from one author to another. Fe I was hardened by Turbatte,[31] following the procedure of Prönnecke *et al.*,[32] Fe II hardening is based on the work of Vascon and Doan,[33] and the description of Fe III hardening can be found in an article discussing the role of Cu in displacement cascades.[34]

Repulsive branches can be characterized by two parameters: their range and their stiffness. If one denotes the range by ρ, the stiffness may be defined by

$$h=\left|\nabla_{r=\rho} V(r)\right|, \tag{2.8}$$

where $V(r)$ is the potential function. For close encounter potentials, a natural choice for characterizing the range is the screening length which is, typically, a fraction of the Bohr radius. In practice, the interaction energies associated with such small distances are in the 10 keV range. In atomic collision cascades, however, the largest amount of encounters occur at much lower energies and such small distances are thus not quite representative. Similarly, as MD potentials are concerned, first-neighbor distances between atoms at their

TABLE I. Characteristics of the three Molière potentials matched to the repulsive branch of the EAM potentials used, in the 0–200 eV energy region, compared to the characteristics of the corresponding three pair potential components.

	Molière II	Molière III	Molière I	Fe II	Fe III	Fe I
Screening length a_{12} (Å)	0.0653	0.0781	0.112	-	-	-
Range ρ at 30 eV (Å)	~1.05	~1.2	~1.6	~1.03	~1.19	~1.57
Stiffness h (eV/Å) at 30 eV	~220	~180	~120	~140	~140	~140

equilibrium sites are also not quite representative of collision cascade situations. Therefore, in what follows, the range of repulsive branches will be arbitrarily characterized as the distance at which the interaction energy is 30 eV. In the case of the close encounter potentials used in the BCA, there is a univocal relation between range and stiffness. The shorter the range, the larger the stiffness, whatever the interaction energy. The situation is different, by construction, for the repulsive branches of many-body potentials. For the EAM potentials used in the present work, the stiffnesses at 30 eV are equal while the ranges are different as can be seen Table I.

We adjusted the screening length of the Molière potentials so as to be close to the repulsive branches of the three EAM interatomic potentials in the 0–200 eV energy range (see Fig. 2). Table I summarizes the characteristics of the three EAM pair components and of their three ''corresponding'' BCA potentials.

B. Full molecular dynamics and its binary collision approximation

Full MD has the advantage to model the time evolution of a box of atoms as a whole. It may be viewed as a method of solving numerically and stepwise in time a large set of coupled simultaneous equations of motion and suitable algorithms allow to make the computer time required therefore only linearly growing with the number of particles involved. The MD code we use, DYMOKA, is a slightly modified version of CDCMD (Ref. 35): a user-oriented code developed to perform Metropolis Monte Carlo and classical MD modeling. The Newton equations of motion are integrated using a fifth-order GEAR predictor-corrector algorithm. The neighbor search is done through a linked cell method combined with a Verlet list.[36] This makes the code fully linear with the number of atoms. The interatomic potentials are tabulated and developed according to the EAM.[19] In order to simulate displacement cascades, the following commonly used approximations are made. The effect of electron excitation is ignored. No damping forces are applied to the boundary atoms. Periodic boundary conditions (PBC's) are used with a choice of the simulation box size depending upon the energy of the PKA. At the beginning of the simulation, the system of particles is let to equilibrate for 5 ps. More detail on the procedure can be found in a previous article.[6]

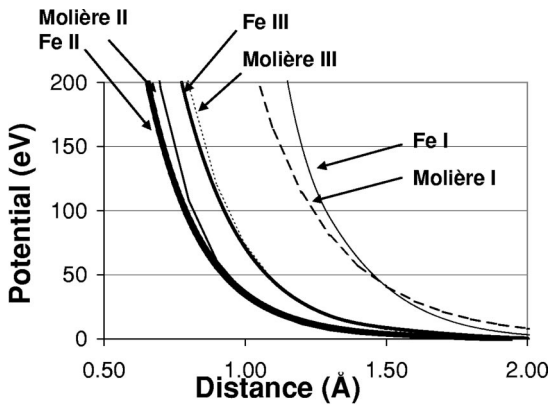

FIG. 2. Repulsive pair components [ϕ in Eq. (2.1)] of the three MD potentials compared to the three Molière potentials adjusted in the 0–200 eV energy range.

The MARLOWE program was used to model atomic collision cascades in the binary collision approximation. The model is described through an extensive literature. A basic reference is given by Robinson.[37] Collision cascades in bulk materials are described as sequences of binary encounters between which atoms move freely along their scattering asymptotes. Individual collisions are governed by pair potentials that may have an attractive component.[38] The potential function is used to estimate the scattering angle and the time integral in each binary collision. Integration is achieved by means of a quadrature with tunable accuracy. The scattered and recoil atomic momenta, as well as the exit asymptote positions, are calculated using that scheme. In the present study, electron excitations have not been modelled. The binary collisions are chronologically ordered. The number of collisions undergone by the moving atoms is limited by a maximum impact parameter value selected by the user. In the present study for iron, it is chosen a little larger than the first neighbor distance. Energy parameters are available to model the binding of atoms to their lattice site and to cutoff their trajectories. In a collision, a target atom is set into motion if it receives a kinetic energy higher than the sum of its binding energy and a cutoff energy threshold. It stops when its kinetic energy falls below this theshold. When this happens, if the recoiling atom receives sufficient energy to be set into motion, the projectile is considered to replace the target at its lattice position. Otherwise, it is considered as an interstitial. In the BCA simulations used for the present discussion, the cutoff energy threshold E_{th} and the binding energy of the atoms to their lattice sites are both taken as equal to the cohesive energy in iron. In replacement collisions, however, the binding energy is either considered as zero or matched to MD results as shown below and discussed for fcc and $L1_2$ structures.[12] This way, collision statistics and displacement cascade morphologies, as obtained by full MD and its BCA, are in good aggreement.[3,4]

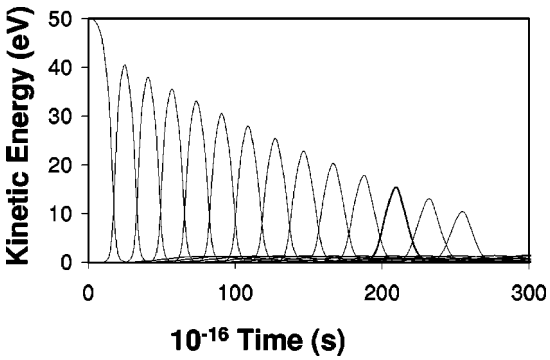

FIG. 3. RCS's along the ⟨100⟩ direction. MD simulation with Fe III EAM potential. The PKA initial energy was 50 eV.

C. Cascade morphologies

Component analysis has been used in this work to characterize the cascade size. This technique associates one ellipsoid to each individual displacement cascade, which accounts for its spatial extension and its morphology on the basis of its intrinsic characteristics.[39] It is thus useful for making comparisons between cascades. The information provided by this method is the direction of three orthogonal axes that are associated to the spatial point defect distribution and the variance of this distribution projected onto them. The major axis has the direction maximizing the variance, the second maximizes the variance of the distribution projected onto a plane perpendicular to the first, and the third one has the direction minimizing this variance. In what follows, subcascade formation is not taken into account. Therefore each cascade is associated with one single ellipsoid which accounts for its spatial extension. This ellipsoid defines the vacancy cascade core volume from which the vacancy density is derived. Statistics have been accumulated in the BCA over 1000 cascades.

D. Characteristics of the MD potentials

Before going into the details of the BCA results, we notice that Fig. 1(a) exhibits very long RCS's. Long RCS's are thus possibly a feature of atomic collision cascades. Since RCS's have been shown to be important in the creation of residual point defects in Fe,[14] we present in this section some characteristics of the MD potentials related to the RCS production: mainly the energy losses during collisions and the focusing thresholds.

The amount of energy lost during the collisions plays a decisive role on the RCS length. Figure 3 shows an example of the variation with time of the kinetic energy in a ⟨100⟩ replacement sequence at 0K for Fe III in MD. The figure displays a series of curves, each one containing one peak. Each curve corresponds to one atom in the replacement sequence. The first atom (which will be referred to as the PKA for the sake of clarity) is initiated with an energy of 50 eV. Its kinetic energy decreases while it exits from its potential well and interacts with a ring of neighbor atoms at the same time as with its first neighbor along the replacement direction (here ⟨100⟩). The next peak corresponds to the temporal dependence of the kinetic energy of the PKA's first neighbor in the direction of the replacement sequences, the third peak to that of the PKA's second neighbor (or the second atom first neighbor along the replacement collision direction), and so on. The energy loss along the collision sequence appears to be rather constant. This constant energy loss was also found in fcc metals,[12] and the mechanism was identified. The energies involved in RCS's are typically of the order of a few ten eV and they are conveniently viewed as sequences of distant binary events that overlap in time. Using this approach, one can determine the position of the turning point of the projectile in a RCS, which is reached at midcollision with the next atom in the row. This turning point, corresponding to the distance of closest approach, is typically close to the intersection point between the row axis and the transverse plane determined by the ring of atoms neighboring the row. Therefore, the interaction with this ring and the next atom in the row are not separated in time. It was found that, for this reason, the ring contributes to slow down the projectile on its path toward the ring.[12] Its acceleration after passing the ring is prevented by the interaction with the next atom in the ring in such a way that the kinetic energy lost on the path toward the ring cannot be restored, hence the energy loss. From this picture, it comes out that the energy loss depends on two factors: namely, the potential range, on which depends the location of the turning point with respect to the ring, and the potential stiffness, on which depends the strength of the interaction with the ring. Table II presents the energy loss per collision along the ⟨100⟩ and ⟨111⟩ directions for the three EAM potentials. These results indicate that it is the shortest range potential (Fe II) which induces the largest energy losses per collision in the sequences, no matter the directions.

TABLE II. Total energy loss (at 0 K) per collision (eV) along ⟨100⟩ and ⟨111⟩ for the three MD potentials.

	Fe II	Fe III	Fe I
⟨100⟩ replacement sequence	3.05	2.52	1.668
⟨111⟩ replacement sequence	1.56	0.75	0.401

It is known that, whatever the potential function, low-energy collision sequences tend to focus momentum along close-packed directions while focusing is not possible at high energy. A threshold energy between the two regimes can be determined as was already done in the past by MD,[40,41] as well as analytically.[42] A detailed analysis is given by Robinson.[11] Table III presents the focusing threshold along ⟨111⟩ and ⟨100⟩ at 0 K for the three MD potentials. The thresholds were determined using the method derived by Erginsoy and co-workers.[41] In a perfect lattice, one atom is given a momentum along one direction. The ratio between the angle of the incident atom with respect to the row axis and that of its neighbor (along the chosen direction) at their maximum kinetic energy is determined for various momentum and incident angle. The focusing threshold is the first energy value for which this ratio is larger than one. As observed by Erginsoy *et al.*,[41] the focusing threshold at 0 K is not very sensitive to the angle between the momentum of the initial particle in the sequence and the row axis.

TABLE III. Focusing threshold (eV) at 0 K along ⟨100⟩ and ⟨111⟩ for the three MD potentials.

Incident angle (deg)	Fe II	Fe III	Fe I	Erginsoy *et al.* [a]
		⟨100⟩		
11.31	36	26	26	
2.86	36	28	24	18
0.63	36	28	24	
		⟨111⟩		
7.33	22	20	24	
5.77	20	20	24	28
1.84	20	18	22	

[a]Reference 41.

III. RESULTS

We now investigate, in a systematic manner, the influence of the potential stiffness and range on the amount and length of RCS's created. Such a study is conveniently done in the BCA.

A. Potential range and stiffness influence on the RCS production

1. Influence of the potential on the energy losses during the RCS production

In the BCA, neither the dynamic overlap in the RCS's nor the many-body potential component are properly accounted for; however, consistently with the picture developed in the previous section, Table IV shows that the stiffer the repulsive potential—and thus the shorter the potential range—the more separated the interaction with the ring and the next neighbor and the smaller the energy loss.

It is interesting to notice that the difference in the energy losses between the three MD potentials is not as pronounced as the difference between their corresponding Molière potential when used in the BCA. In contrast with screened Coulomb potentials, for which the stiffness is a monotonous function of the range, the MD potentials are usually constructed from different functions spliced together (see, for instance, Ref. 43 or Appendix A of Ref. 44), and both potential characteristics are independent parameters.

2. Influence of the potential on the number of RCS's

Another aspect of RCS production is the influence of the potential characteristics on their production efficiency and their length. Figure 4 shows the mean number of RCS's produced and their length distribution as functions of the screening length in the Molière potential. It indicates that the number of RCS's is a decreasing function of the screening distance and thus of the range of the potential. In other words, the larger the contribution of the environment, the lower the number of RCS's. The reason why the number of RCS's is a decreasing function of the potential range is not obvious and requires a better understanding of the conditions for RCS production. The explanation comes out an analysis of the focusing energy threshold.

TABLE IV. Energy loss (at 0 K) per collision (eV) along ⟨100⟩ and ⟨111⟩ and focusing threshold for the three Molière potentials mimicking the three MD potentials.

	Molière II	Molière III	Molière I
⟨100⟩ replacement sequence	0.04	0.5	13.998
⟨111⟩ replacement sequence	0.003	0.07	5.567
Focusing threshold (eV)	~7	~20	~80

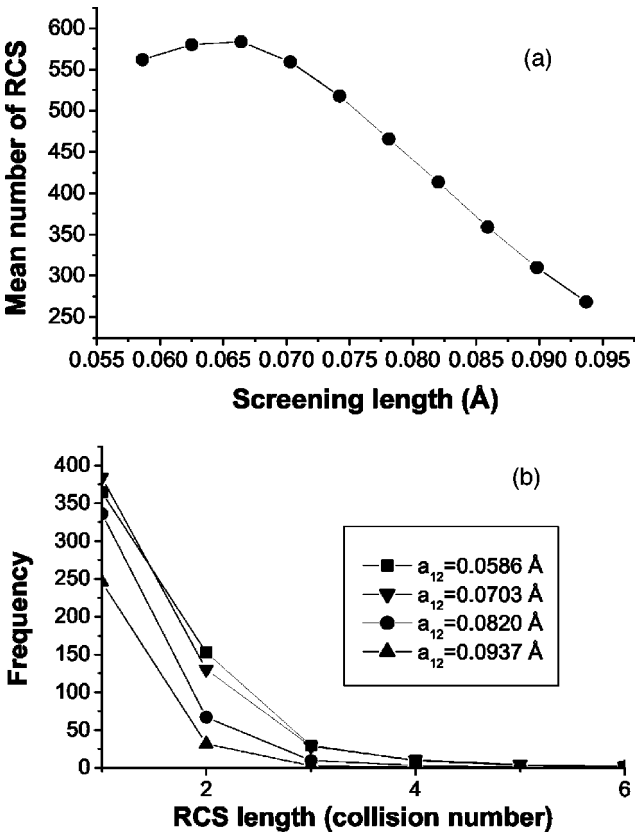

FIG. 4. Influence of the screening length in the Molière potential on the RCS's. (a) Mean number of RCS's as a function of the screening length. (b) RCS length frequency distribution for different values of the screening lengths in (a).

3. Influence of the potential on the focusing thresholds

The focusing thresholds for the three Molière potentials are reported in Table IV. Since in the BCA the asymptotes of particle motion are well known, to evaluate momentum directions and, thus, focusing thresholds is rather straightforward. As can be seen in Fig. 5, the focusing threshold varies significantly with the screening length. The higher the screening length, the higher the focusing threshold and the higher the energy at which focused sequences will take place.

The ratio between the focusing threshold energy (i.e., the energy of the first atom of the RCS's for which focusing starts) and the energy loss per collision gives an indication of the length of RCS's which will be produced in the cascades.

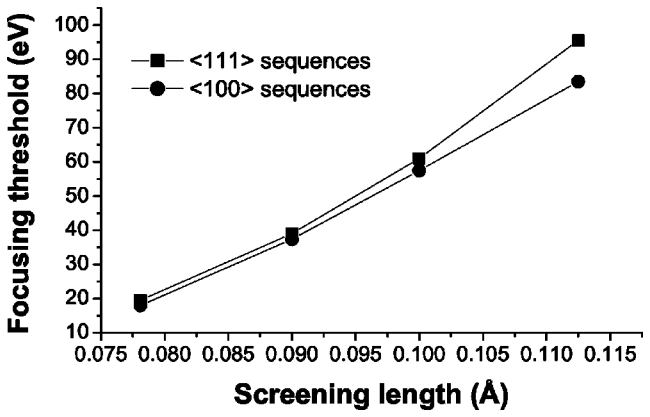

FIG. 5. Focusing threshold as a function of the screening length in the Molière potential. Results are shown in cases where the initial direction makes a small angle with a ⟨100⟩ and a ⟨111⟩ direction.

Considering Table IV and Fig. 5, it appears very clearly that even though Molière II has a lower focusing threshold than the other potentials, it should produce longer RCS's than the other two potentials. More generally, the higher the screening length, the longer the RCS's should be, despite lower focusing thresholds. This is what is observed in Fig. 4, even if the RCS's produced are much shorter than what could be expected from the energy loss and focusing threshold given in Table IV. The fact that the RCS's are predicted short whatever the potential stiffness or range is investigated in more detail elsewhere.[14]

It comes out of this first part of the discussion that the shorter range or the stiffer the BCA potential in the 0–200 eV range (it is not at this point possible to determine which parameter is the most prevalent), the lower the focusing threshold and the more important the RCS production. This is confirmed by the results of Table V and Fig. 7, below (which are discussed in more details in Sec. III B 1) which indicates that a Born-Mayer potential adjusted so that it is close to the Molière potential in the 0–200 eV produces similar energy losses, similar focusing threshold and thus similar RCS length and number as the Molière potential.

We now turn to the other important difference in the cascade morphologies presented Fig. 1: their density. The displacement cascades obtained with the MD potential Fe II are very lose and dilute, while the cascades produced with the other two potentials are much more compact. BCA potentials are thus used to seek for an explanation of these behaviors.

B. Cascade expansion

We now address the question of what determines the cascade expansion. In this aim we compare the predictions of Molière and Born-Mayer potentials. The interest comes from the fact that, at short range enough, the Molière potential is always stiffer than the Born-Mayer potential while they match at larger distances. This will allow to single out the role of close encounters in the cascade expansion.

1. Adjustment of the two potentials

The screening parameter in the Born-Mayer potential is adjusted the same way as was done with the Molière potential, namely, by matching to the MD potentials in the energy region involved in RCS's, typically below 200 eV. For each MD potential we thus dispose of two pair potentials similar in the 0–200 eV region, but very different at higher energies. Figure 6 displays the two pair potentials mimicking Fe III.

TABLE V. Energy loss (at 0 K) per collision (eV) along ⟨100⟩ and ⟨111⟩ and focusing threshold for the Molière potential and Born-Mayer potential mimicking Fe III.

	Energy loss per collision (eV)	
	Molière III	Born Mayer III
⟨100⟩ replacement sequence	0.5	0.43
⟨111⟩ replacement sequence	0.07	0.05
Focusing threshold (eV)	~20	~19.5

For these two potentials, the energy losses in RCS are only slightly different as can be seen in Table V. This fact is consistent with the results of Fig. 7 which shows that both series of potentials predict similar RCS numbers and lengths. These results indicate that, as expected, most RCS's develop in the energy range of good matching between Molière and Born-Mayer potentials. One may add that in all the BCA results investigated, no replacement was detected at energies higher than 200 eV.

2. Cascade volumes and densities

This potential adjustment allows us to address the question of which factors determine the cascade volumes, mor-

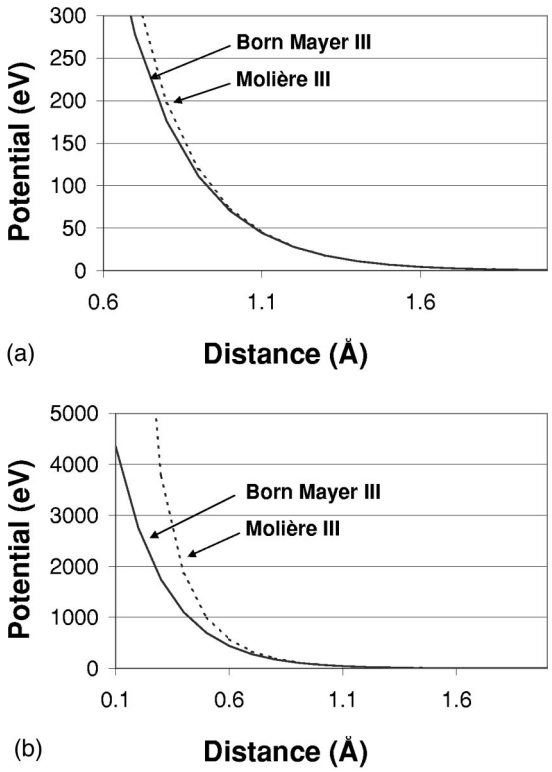

FIG. 6. The Molière and the Born-Mayer potentials matched to the repulsive branch of the Fe III. (a) Complete energy range and (b) RCS formation energy range.

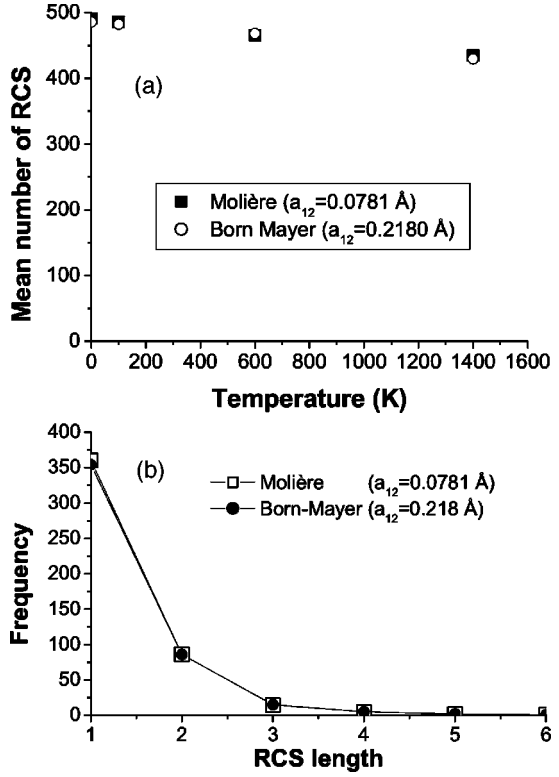

FIG. 7. RCS length estimates with the Molière and the Born-Mayer potentials matched to the repulsive branch of the Fe III (a) mean number of RCS at 0 K, 100 K, 600 K, and 1400 K, (b) frequency distribution at 600 K.

phologies and densities. In Fig. 8, cascade volume distributions are shown, as obtained in the BCA with the Molière III and the BM III potentials. The distributions are both quite broad. Their full width at half maximum is equal to or larger than the modal volume value. It however comes out that, despite the good potential matching in the 200 eV range and below, the cascade expansion with the BM potential is generally much larger than the one obtained with the Molière potential which is stiffer and larger ranged at high energy.

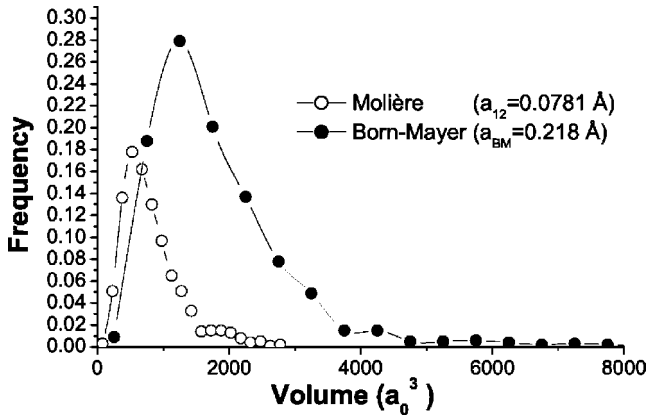

FIG. 8. Displacement cascade volume distributions obtained with the Molière (open circles) and the Born-Mayer (solid circles) potentials matched to the repulsive branch of the Fe III EAM potential.

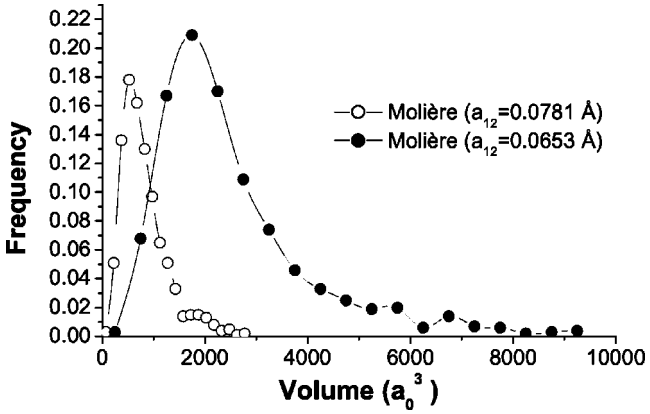

FIG. 9. Displacement cascade volume distributions obtained with the Molière potential matched to the repulsive branch of the Fe II (solid circles) and Fe III (open circles) potentials.

First, since the focusing threshold is in the energy range of good matching between the potentials, they do not play a significant role in the cascade expansion. Second, Fig. 8 tends to indicate that the potential with the shortest range at high energy predicts, the less compact cascades. Indeed the volumes presented in Fig. 8 are obtained by adjusting the vacancy-interstitial recombination distance in such a way that the numbers of Frenkel pairs predicted are similar. Cascades with smaller volumes are thus denser. The same trend is observed for volumes obtained with two different Molière potentials, mainly the one mimicking Fe III and the one mimicking Fe II. Molière III is stiffer and larger range than Molière II and it predicts smaller and thus denser cascades (Fig. 9). These results suggest a possible interpretation of the cascade morphologies as displayed Fig. 1. The MD potential Fe II is the shortest range among the three Fe potentials and it produces the least dense displacement cascades. In dense cascades, RCS's are more likely to be interrupted than in dilute cascades, and the interstitials created by the RCS's, remaining in more disordered zones, are then more likely to recombine than when they are created away from the cascade core. Thus the cascade density appears to play an important role in the number of long RCS's and thus in the number of post-recombination surviving Frenkel pairs. This study indicates that the high-energy range (above 200 eV) of the potential strongly influences the cascade volume and thus its density. The cascade evolution can be investigated more comprehensively by considering the energy threshold E_{th} defined in Sec. II B as a parameter.

This displacement threshold is conveniently tuned in the BCA and cascade volume distributions can be constructed. In Fig. 10, we show the results obtained for $E_{th}=E_{PKA}/2^n$, where n is varied from $n=5$ to $n=10$, and E_{PKA} is the initial energy of the PKA. Since one relevant characteristics of these distributions is the modal volume, denoted here as Ω_M, its value can be evaluated as a function of n. The same can be done with the anisotropy factor distributions. Ω_M and the modal anisotropy factor are represented as functions of n in Fig. 11. From this figure, it is seen that, at the highest energies, the volume increases close to linearly with n and, for $n \leqslant 7$ ($E_{th}=150$ eV for a 20 keV PKA), it thus scales

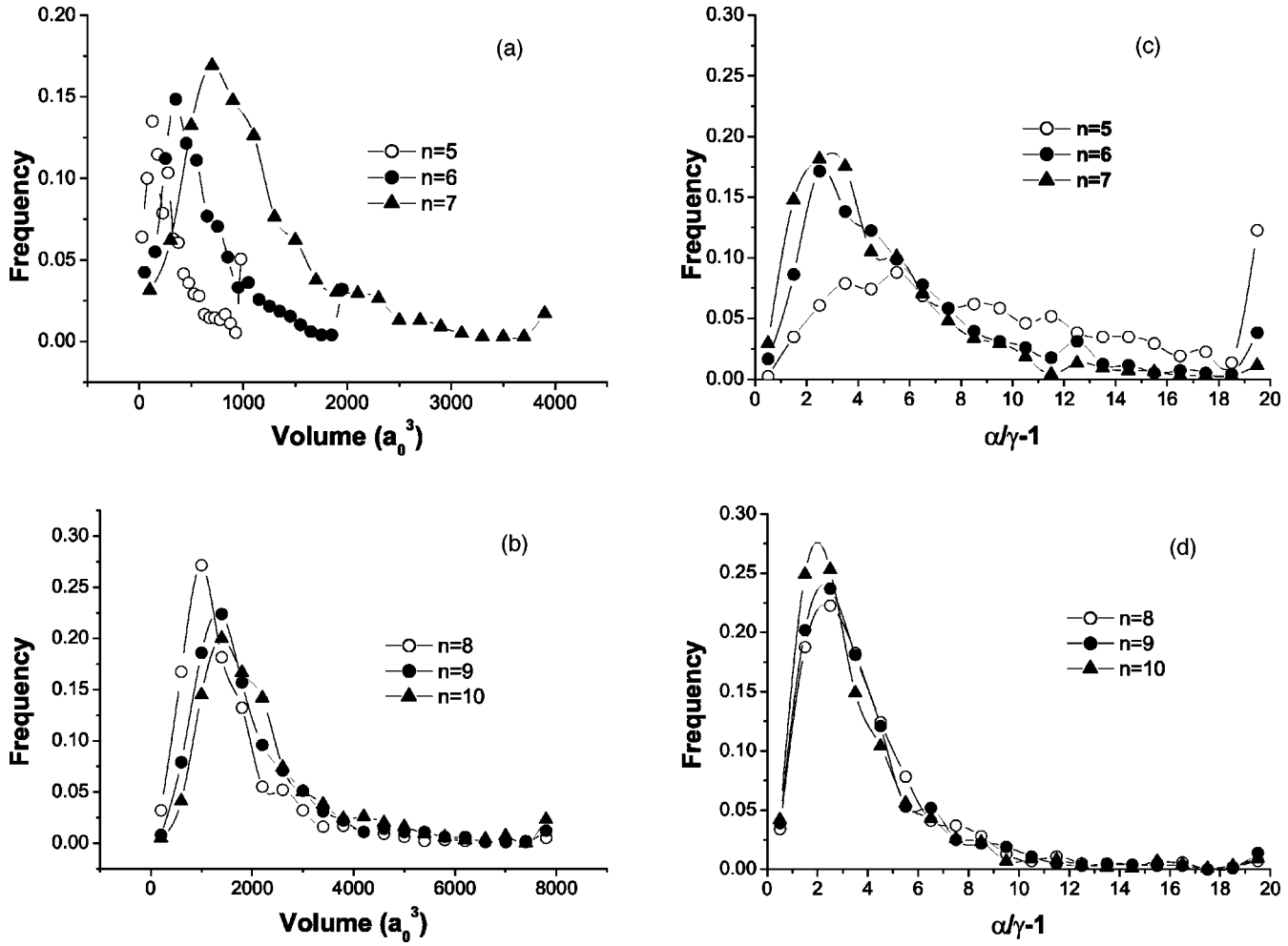

FIG. 10. Cascade volume (a),(b) and anisotropy factor (c),(d) distributions for different values of the cutoff energy threshold E_{th}. The distributions are represented for $E_{th}=E_{PKA}/2^n$ with n varying from 5 to 10. The last channel in each distribution accumulates all the higher values. The initial energy of the PKA, E_{PKA}, is 20 keV.

with ν. Since the number of displaced atoms also increases linearly with n, the cascades expand at constant displacement density. The expansion does not proceed for $n \geqslant 9$ ($E_{th}=40$ eV for a 20 keV PKA). Similarly, the anisotropy factor is a faster decreasing function of n in the highest-energy range, which means that the lowest-energy displacements contribute to self-similar expansion while high-energy displacements contribute to elongation. Since neither the volume nor the anisotropy are significantly affected for $n \geqslant 9$, lower-energy displacements can only contribute to cascade densification. This energy is somewhat above the focusing threshold and RCS's thus mainly contribute to densification. Furthermore, in the BCA calculations presented in this work, the displacement threshold used is set equal to the cohesive energy (4.28 eV). Hence, according to a Kinchin-Pease argument, the number of atoms that have moved above this threshold value is $\nu_{BCA}=1870$ (the number of atoms displaced at the peak in MD cascades is about 4 times larger). Since the cascades are not expanding further than for $n=9$, which corresponds to $\nu \cong 200$, it comes out that the cascade volumes are determined by 10% $[\nu(n=9)/\nu_{BCA}]$ highest-energy recoils in the cascade.

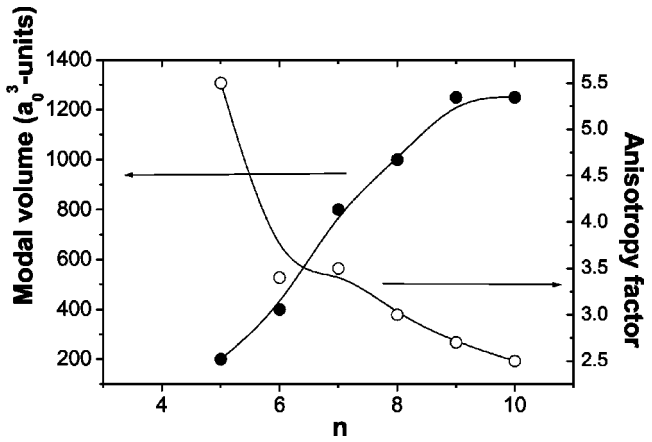

FIG. 11. Modal cascade volumes and anisotropy factor as a function of n, estimated from the results given in Fig. 10.

IV. CONCLUSIONS

We have investigated the influence of different parts of the repulsive potential in the RCS production and cascade

expansion as MD simulations pointed out that striking differences are possible. As the Marlowe package provides a large variety of pair potential functions and allows one to adjust their parameters very conveniently, we explored in a systematic and statistical manner the influence of the range and stiffness of the BCA potentials on the RCS frequency distributions and lengths. From these results, the RCS model used in the BCA was carefully tuned on the basis of the energy loss estimated by full MD. The energy range for RCS production is 0–200 eV and similar amounts of RCS are generated by repulsive potentials exhibiting similar stiffness and range in this energy range. The shorter range or the stiffer the potential in the BCA, the lower the focusing threshold and the more important the RCS production. However, the RCS production is not the only parameter governing the primary damage and this work points out that the cascade spatial extension and its density, i.e., the number of Frenkel pairs produced per unit volume, seem also to be dependent on the potential range at higher energies. We suggest that the defect density and thus the disorder may significantly interfere with the RCS propagation, especially in the case of long sequences. It was also shown in this study that the cascade spatial expansion is determined by a limited amount of highest-energy recoils. The cascade extension and density and not only the RCS production are thus to be considered to evaluate the primary damage.

ACKNOWLEDGMENT

This work is part of the REVE (virtual reactor) project which aims at simulating the irradiation effects in structural materials.

[1] S. Jumel, C. Domain, J. Ruste, J.C. van Duysen, C.S. Becquart, A. Legris, P. Pareige, A. Barbu, E. van Walle, R. Chaouadi, M. Hou, G. Odette, R. Stoller, and B. Wirth, J. Test. Eval. **30**, 37 (2002).

[2] H.L. Heinisch, B.N. Singh, and T. Diaz de la Rubia, J. Nucl. Mater. **212-215**, 127 (1994).

[3] M. Hou and Z-Y. Pan, Radiat. Eff. Defects Solids **142**, 483 (1997).

[4] A. Souidi, M. Hou, C.S. Becquart, and C. Domain, J. Nucl. Mater. **295**, 179 (2001).

[5] M. Hou, A. Souidi, and C.S. Becquart, J. Phys.: Condens. Matter **13**, 5365 (2001).

[6] C.S. Becquart, C. Domain, A. Legris, and J.C. van Duysen, J. Nucl. Mater. **280**, 73 (2000).

[7] T. Diaz de la Rubia, R.S. Averback, Hornming Hsieh, and R. Benedek, J. Mater. Res. **4**, 579 (1989).

[8] G. Leibfried, J. Appl. Phys. **30**, 1388 (1959).

[9] R.S. Nelson and M.W. Thompson, Proc. R. Soc. London, Ser. A **259**, 458 (1961).

[10] H.H. Andersen and P. Sigmund, K. Dan. Vidensk. Selsk. Mat. Fys. Medd. **34**, 15 (1966).

[11] M.T. Robinson, in *Sputtering by Particle Bombardment*, edited by R. Behrish, Topics in Applied Physics Vol. 47 (Springer-Verlag, Berlin, 1981).

[12] M. Hou, Nucl. Instrum. Methods Phys. Res. B **187**, 20 (2002).

[13] A. Souidi, A. Elias, A. Djaafri, C.S. Becquart, and M. Hou, Nucl. Instrum. Methods Phys. Res. B **193**, 341 (2002).

[14] M. Hou, A. Souidi, and C.S. Becquart, Nucl. Instrum. Methods Phys. Res. B (to be published).

[15] W.J. Phythian, R.E. Stoller, A.J.E. Foreman, A.F. Calder, and D.J. Bacon, J. Nucl. Mater. **223**, 245 (1995).

[16] F. Gao, D.J. Bacon, P.E.J. Flewitt, and T.A. Lewis, J. Nucl. Mater. **249**, 77 (1997).

[17] C.S. Becquart, C. Domain, A. Legris, and J.C. van Duysen, in *Multiscale Modelling of Materials*, edited by G.E. Lucas, L. Snead, M.A. Kirk, Jr., and R.G. Elliman, MRS Symposia Proceedings No. 650 (Materials Research Society, Pittsburgh, 2001), p. R3.24.

[18] F. Ducastelle, J. Phys. (Paris) **31**, 1055 (1970).

[19] M.S. Daw and M.I. Baskes, Phys. Rev. Lett. **50**, 1285 (1983).

[20] P. Gombàs, in *Handbuch der Physik*, edited by S. Flügge, (Springer, Berlin, 1956), Vol. 36, p. 109.

[21] G. Molière, Z. Naturforsch. A **2**, 133 (1947).

[22] O.B. Firsov, Sov. Phys. JETP **36**, 1076 (1959).

[23] J. Lindhard, V. Nielsen, and M. Scharff, K. Dan. Vidensk. Selsk. Mat. Fys. Medd. **36**, 10, 1 (1968).

[24] J.F. Ziegler, J.P. Biersack, and U. Littmark, *Stopping Powers and Ranges of Ions in Matter* (Pergamon, New York, 1985), p. 25.

[25] S.T. Nagakawa and Y. Yamamura, Radiat. Eff. **105**, 239 (1988).

[26] M.T. Robinson, K. Dan. Vidensk. Selsk. Mat. Fys. Medd. **43**, 28 (1993).

[27] R.J. Harrison, A.F. Voter, and S.P. Chen, in *Atomistic Simulation of Materials—Beyond Pair Potentials*, edited by V. Vitek and D.J. Srolovitz (Plenum, New York, 1989), Vol. 219.

[28] M.I. Haftel, T.D. Andreadis, J.V. Lill, and J.M. Eridon, Phys. Rev. B **42**, 11 540 (1990).

[29] G. Simonelli, R. Pasianot, and E.J. Savino, in *Materials Theory and Modelling*, edited by J. Broughton, P.D. Bristowe, and J.M. Newsam, MRS Symposia Proceedings No. 291 (Materials Research Society, Pittsburgh, 1993), p. 567.

[30] F. Maury, M. Biget, P. Vajda, A. Lucasson, and P. Lucasson, Phys. Rev. B **14**, 5303 (1976).

[31] J.C. Turbatte, Master of Science thesis, Université de Marne la vallée, 1995.

[32] S. Prönnecke, A. Caro, M. Victoria, T. Diaz de la Rubia, and M.W. Guinan, J. Mater. Res. **6**, 483 (1991).

[33] R. Vascon and N.V. Doan, Radiat. Eff. Defects Solids **141**, 375 (1996); R. Vascon, Ph.D. thesis, Université Paris XI, 1997.

[34] C.S. Becquart, C. Domain, J.C. Van Duysen, and J.M. Raulot, J. Nucl. Mater. **294**, 274 (2001).

[35] A C version of CDCMD can be found at http://www.ims.uconn.edu/centers/simul/index.htm#xmd.

[36] M.P. Allen and D.J. Tildesley, *Computer Simulation of Liquids*, (Clarendon Press, Oxford, 1986).

[37] M.T. Robinson, Phys. Rev. B **40**, 10 717 (1989).

[38] M.T. Robinson, Radiat. Eff. Defects Solids **141**, 1 (1997).

[39] M. Hou, Phys. Rev. B **31**, 4178 (1985); Phys. Rev. A **39**, 2817 (1989).
[40] J.B. Gibson, A.N. Goland, M. Milgram, and G.H. Vineyard, Phys. Rev. **120**, 1229 (1960).
[41] C. Erginsoy, G.H. Vineyard, and A. Englert, Phys. Rev. **133**, A595 (1964).
[42] R.H. Silsbee, J. Appl. Phys. **28**, 1246 (1957).
[43] A.F. Calder and D.J. Bacon, J. Nucl. Mater. **207**, 25 (1993).
[44] C.S. Becquart, C. Domain, J.C. van Duysen, and J.M. Raulot, J. Nucl. Mater. **294**, 274 (2001).